Effects on the compressive strength of cement-stabilized rammed earth blocks with varied content of buffelgrass-based fibers in wet-dry conditions

Federico Pederson[1], Reuel Florendo[1], Saleh Ali Khawaja[1], Kirk Dimond[2]* and Hee-Jeong Kim[1]*

[1]Department of Civil and Architectural Engineering and Mechanics, University of Arizona, Tucson, AZ, United States, [2]School of Landscape Architecture and Planning, University of Arizona, Tucson, AZ, United States

Stabilized rammed earth blocks have been an alternative building material around the world due to their cost efficiency, low embodied energy, and environmental footprints. However, the lower compressive strength and resistance to wearing limits their use in comparison to higher-cost alternatives. The integration of fibers in rammed earth blocks has been a promising technique for enhancing their properties. In this research, the viability of buffelgrass as a reinforcing fiber in stabilized earth blocks was determined. The buffelgrass was incorporated into the mix up to 5% by weight for samples with the increment of 1% for each mix and the durability was determined under wet and dry conditions. In addition, the influence of the buffelgrass on the compressive strength was observed and the optimum content was determined. The morphological characteristics were observed using SEM imaging of the rammed earth and fiber interaction at a fracture surface. The results showed the inclusion of buffelgrass helps the wear resistance of the earth blocks when exposed to wet-dry conditions as well as slightly improving the compressive strength of the material after dry and wet curing.

KEYWORDS

rammed earth, cement stabilized rammed earth, plant fibers, buffelgrass, fiber reinforced

1 Introduction

OPC based concrete and fired clay bricks are both important materials in modern construction. However, in recent years a larger focus has been placed on how the production of concrete contributes to about 8% of the total carbon footprint per year (Editorial, 2021). Fired clay bricks have an estimated global production of 1390 billion units per annum with roughly 70%–80% of this being fired in a kiln (Murugan et al., 2022; Wang et al., 2022). The traditional process of manufacturing kiln bricks is energy-intensive due to the high temperatures needed for firing (500°C–900°C depending on kiln type) (Javed et al., 2020; Mañosa et al., 2022). The estimated CO_2 emission from the thermal activation of a single kiln brick is 162 g–171 g (Xin et al., 2023). Additional emissions from brick kilns are comprised of fine dust particles, hydrocarbons, SO_x, NO_x, CO, fluoride compounds, and a small number of carcinogenic dioxins (Skinder et al., 2014). The average amount of particulate matter is 0.46–1.4 kg and SO_2 is 0.52–5.9 kg per 1,000 bricks, contributing

to local air pollution problems (Skinder et al., 2014). To combat these problems alternative building materials have been explored such as stabilized rammed earth blocks (SREB).

The main components of SREBs are soil, stabilizer, water, and in some cases a reinforcing fiber (Liu et al., 2022). The availability of the raw material paired with only containing 15%–25% of the embodied energy of an equivalent kiln fired brick, makes SREB bricks an eco-friendly alternative for construction (Venkatarama Reddy & Prasanna Kumar, 2010; Elahi et al., 2021). However, there are limitations on the compressive strength, pore water stability, and durability of SREB bricks which limit its competency as a building material (Liu et al., 2022). To help address this, plant fibers have been used as a sustainable method to improve SREB performance.

A wide range of different plant fiber types can serve as a supplementary constituent of earth construction to address its specific limitation. A comprehensive review on Plant aggregates and fibers in earth construction materials is presented by Laborel-Préneron et al. Giroudon et al. (2019) introduced 3% and 6% barley and lavender straws as a bio aggregate into earth brick with the lavender straws favoring the adhesion of clay and enhanced compressive strength and durability properties were achieved with 3% of lavender straw in the mix (Giroudon et al., 2019). Microstructural investigation showed that the presence of cement in mix increases the calcite peaks and reduce the porosity hereby improving the strength and durability properties (Laborel-Préneron et al., 2016; Raavi and Tripura, 2020a).

Buffel grass (BF), or *Cenchrus ciliaris*, grows widely in tropical and sub-tropical regions of the world due to their tolerance towards drought and capacity to withstand heavy grazing (Marshall et al., 2012). Introduced in the early 1930s as a fast-growing grass for grazing cattle, BF has become a major issue for the southwestern United States. The US Department of Interior reported a 35% annual growth in BF in the southern the US, with areas like the Saguaro National Park being covering by 2,000 acres of this grass (U.S. Department of the Interior, 2010). Because the plant is able to dry and revive itself after rain, the grass has the capacity to withstand the harsh environment was categorized as an invasive species in the American southwest (Marshall et al., 2012; U.S. Department of the Interior, 2010). This drying action also increase the wildfire intensity by acting as a combusting fuel (U.S. Department of the Interior, 2010). The rapid and extensive BF growth can result in habitat alteration by out competing native flora for both space and soil resources (U.S. Department of the Interior, 2010; U.S. National Park Service, 2023). Click or tap here to enter text.

In Southern Arizona there has been an interest in the development of low-cost construction materials that use less water and energy to manufacture compared to conventional bricks and concrete. The goal of this study is to determine the viability of fiber reinforced SREBs for use in the context of Southern Arizona. Considering the ecological aspects associated with BF in the context of Southern Arizona, this research investigates: determine the viability of buffelgrass as a stabilizing additive to a cement-SREB, identify the optimum content of buffelgrass, evaluates the compressive strength, and the durability of the resulting SREB under wet-dry cycling. The outcomes of this research act as a method for reducing the material and resource cost of building in Southern Arizona.

2 Materials and methods

2.1 Characterization of soil sample

A Geographic Information System (GIS) analysis informed the soil selection. Soils, as mapped and described in the Soil Survey Geographic Database (SSURGO), were clipped to a 16 km radius for proximity to the University of Arizona campus in Tucson, Arizona United States (testing location). Soil types were narrowed to include types that were described as "Not prime farmland," with low slopes (maximum 5%), and a particle size taxonomy that excluded "coarse" and "skeletal" soils and included "loamy" soils as a qualifier in the particle size description as an attempt to identify soils with a suitable balance in sand, silt, and clay (Nshimiyimana et al., 2020). Yaqui fine sandy loam, 1%–3% slopes was identified as the prevalent soil type meeting the criteria within the 16 km radius boundary. An overlay of publicly accessible lands within the boundary facilitated the identification of the soil collection location. The provided soil sample supplied from this location was limited to 25 kg. This limited the number of samples that could be made for each of the tests described below.

The particle-size distribution by sieve analysis test is used for classification of the soil in accordance with ASTM-D2487, the Standard Practice for Classification of Soils for Engineering Purposes (Unified Soil Classification System) (ASTM, 2020) This is used to determine the approximate particle size in a given sample. This is reported as the percentage by weight of particles that pass through a mesh of a standard size.

Particle size testing is accomplished using a sieve stack and shaker bench. The sieve stack used for this study started at a #4 sieve and increased to a #8, #16, #30, #50, #100, and #200 sieve. The starting weight of each sieve was measured with a bench scale and recorded in Table 1. The starting soil weight of 545.03 g was loaded into the stack and placed in the mechanical shaker. The machine was left to run for 5 minutes, and the weights of each sieve were measured and recorded. A total weight was determined to find the total mass lost over the course of the test.

This data was placed into the Particle Size Distribution graph in Figure 1, which plots the percent finer against the grain size. Based on the Unified Soil Classification System, the information from the Particle Size Distribution curve shows that the soil is well-graded, clean gravel with less than 5% fines.

2.2 Cement and plant fibers

Two stabilizers were used in this experimental study: cement and buffelgrass. The cement used is a blended type 1 and 2 Portland cement conforming to ASTM C150 from CalPortland Cement (ASTM, 2022). The buffelgrass fibers used were pulled from Robles Pass Trails Park, which is located in the Tucson Mountains and managed by Pima County Natural Resources, Parks & Recreation. Their characteristics are listed in Table 2. After natural drying under the Sun, seeds and roots were manually removed to eliminate the

TABLE 1 ASTM-D691 sieve analysis of soil sample.

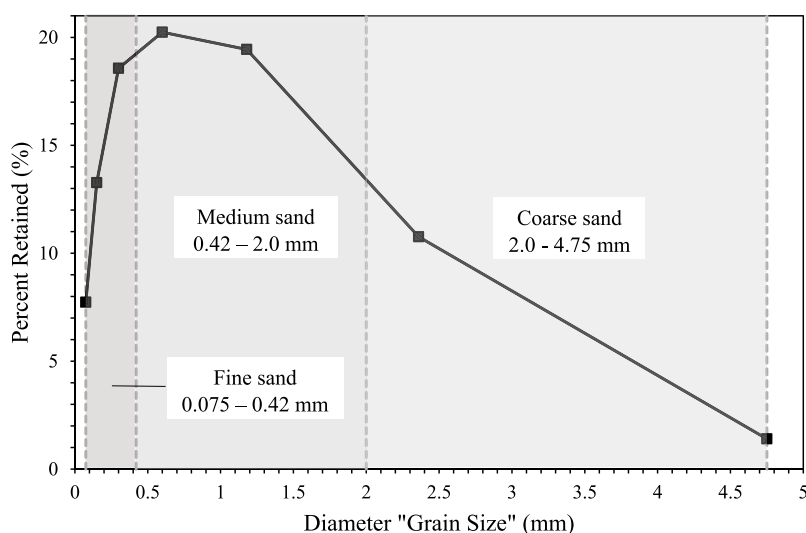| Sieve number	Diameter	Mass of retained soil (g)	Percent	Cumulative percent	Percent
	"Grain size" (mm)		Retained (%)	Retained (%)	Finer (%)
4	4.75	7.63	1.40	1.40	98.60
8	2.36	58.66	10.76	12.16	87.84
16	1.18	105.97	19.44	31.61	68.39
30	0.60	110.32	20.24	51.85	48.15
50	0.30	101.20	18.57	70.41	29.59
100	0.15	72.34	13.27	83.69	16.31
200	0.08	42.13	7.73	91.42	8.58
Base	0.00	47.38	8.69	100.11	−0.11
Lid	0.00	−0.05	−0.01	100.10	−0.10

FIGURE 1
Particle size distribution of base soil material.

TABLE 2 Characteristics of buffelgrass fibers.

Buffelgrass fibers	Length (cm)	Water absorption (g water/g fiber)
	1.25 to 2	1.98

possibility of growth and germination. They were then cut into lengths of 1.5 cm using commercial shears. This length was used as several studies have used fiber lengths that are one-fifth to one-third of the length of the mold (Stazi et al., 2016; Bogas et al., 2023; Koutous and Hilali, 2023). 50 mm cube molds were used to form the final blocks.

TABLE 3 ASTM D698-12 (2021), compaction characteristics at varied moisture content.

	Cylinder 1	Cylinder 2	Cylinder 3	Cylinder 4
Final Moisture Content (%)	0.22	0.26	0.30	0.34
Mass of mold + sample (g)	3678.99	3723.75	3727.12	3618.03
Moist density (kN · m/m³)	0.77	0.79	0.80	0.74
Dry unit weight (kN · m/m³)	7.12	7.20	6.85	6.07

TABLE 4 Formulation of the mix designs tested in this study.

	SP0	SP1	SP2	SP3	SP4	SP5
Earth (kg)	2	1.98	1.96	1.94	1.92	1.90
Cement (% by weight)	10	10	10	10	10	10
Water (% in relation to earth)	27	27	27	27	27	27
Buffelgrass (% in relation to earth)	0	1	2	3	4	5

2.3 Optimum water content testing—Proctor test

The test was done following ASTM D698-12 (2021), the Standard Test Methods for Laboratory Compaction Characteristics of Soil Using Standard Effort (12,400 ftlbf/ft³ (600 kN m/m³)) (ASTM, 2021b). The sample soil had its initial water content determined by oven drying a portion and recording the mass lost overnight at 100°C. Once completed, 2 kg of material were weighted and set aside. The final moisture content percentage was calculated and recorded in Table 3 with the wetted sample being mixed for a minute. A standard Proctor test compaction apparatus and mold were used, where a 2.5 kg weight was dropped a total of 25 times per lift in the pattern listed in the above standard. The mold was filled using three lifts of sample material and the top surface finished with a steel straight edge. The final weight was recorded for each mold and sample with the compacted cylinder being cut into eighths and oven dried. A dry unit weight was recorded in Table 3 for these samples. Using the generated dry unit weight and moisture content graph an optimum moisture value can be estimated.

2.4 Mix design of SREB

To analyze the optimum concentration of the buffelgrass and its influence on the properties of the SREB, five different mix compositions were studied. Table 4 illustrates the mix proportion of each mix type. The aim of the research is to study the influence of buffelgrass content, so the amount of cement was set to 10% by weight for all mixes. Published literature shows a positive impact on compressive strength at this cement concentration when used in SREB applications (Riza and Rahman, 2015; Van Damme and Houben, 2018; Zami et al., 2022). The percentage of the buffelgrass varied from 0% to 5% by weight for samples SP0 to SP5 with the percentage of fibers increasing in steps of 1%. SP0 acts as a control sample with a 0% buffelgrass content. The water content

was determined to be 26% as shown in the results presented later in section 3.1.

2.5 Specimen manufacturing and storage

Test blocks were compacted in 50 mm by 50 mm steel cement cube molds. A starting batch of 2 kg of soil was used as the basis for proportioning the other constituent weights. The cement and soil were weighed out separately before being combined in a mixing bowl and mixed at a medium speed for 1 minute. If any clumps of cement powder were seen the mixer was run for another 30 s. Once the homogeneity in the mix of soil and cement was achieved water was added and mixed until a paste is formed. This produced a thick paste with low workability that stuck to the bowl and gloves. At this point depending on the exact mix design the proportion of fibers were added slowly and hand mixed to prevent damage to the plant fibers in the mechanical mixer.

Compaction was done using a 2.5 kg drop hammer commonly used in the proctor test (ASTM, 2021b), and a 50 mm block of wood to spread the force across the block's surface. This was dropped a total of 10 times with material being added after the fifth and eighth drop to fill the entire volume of the mold. With this set up a compaction effort of 285.2 kN/m² was applied to each block. This was done to maintain a consistent compaction force across all samples while not applying excessive stress to the molds. The samples were allowed to cure in the molds for 24 h before being removed and wrapped in plastic and stored in an enclosed cabinet. These steps were taken to maintain a moist environment so hydration of the cement portion could occur. Photos of the sample preparation process are shown below in Figure 2.

2.6 Uniaxial compression test

Testing of the 50 mm cube samples was conducted after 7 and 28 days of curing. In this test, ASTM C109 (ASTM, 2021a) was used
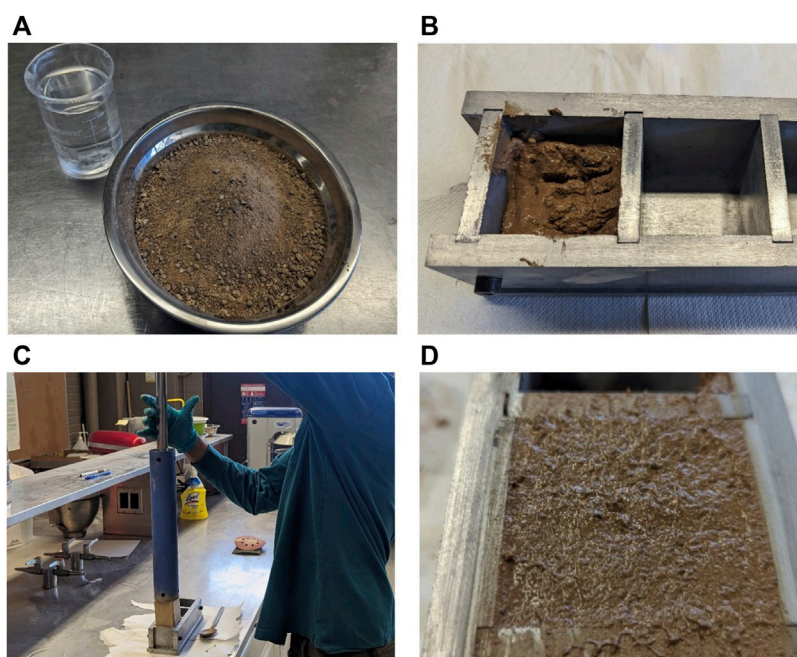
FIGURE 2
This collection of images shows the sample preparation steps to form the 2-inch cube samples. **(A)** The cement and sieved soil were mixed dry using a benchtop mixer, the water and plant fibers were then added and mixed by hand to form paste with even consistency. **(B)** Two layers of paste were added to the steel mold and compacted using the drop hammer. **(C)** Drop hammer and wooden impact spreader block. **(D)** Final compacted sample before curing.

as a guideline. This was done to compare the compressive strength of the samples to other common construction materials such as cement mortars. Two cubes were crushed for each testing session. Sample prep was done by sanding the top and bottom of the samples with 60 grit sandpaper to maintain smooth parallel load surfaces. The cross-section was measured at three points for each dimension and averaged. Once sanded, a cube was loaded into a load frame with the load direction being parallel to the direction of compaction. Loading was conducted at a rate roughly 1332 N/s and stopped after a 20% drop in applied load was noted.

2.7 Water curing test

A water curing test was used to determine if any changes in the mechanical properties of the blocks will occur when the sample is exposed to water over a long period of time. This is important for structures such as embankments or small-scale water works. The test was conducted by placing two blocks in a tank after allowing the samples to be air cured for 7 days. After 14 and 28 days submerged in water the samples were removed and the compressive strength of the material was taken. Compression was conducted with the same equipment and test setup as the uniaxial compression section listed above.

2.8 Wet-dry cycle testing

The wet-dry cycling test was conducted after allowing the sample to cure for 7 days. After this point two cubes had their

average dimensions and dry mass recorded before testing. These were then placed in standing water and left covered for 5 h. These were pulled from the water and placed in an oven set to 115°C for 48 h to drive off any residual water. Once dried, a wire brush was used to scrape any loose powder off the sample. The scrapping action was done by hand with the brush being run vertically down the block's faces twice on each side. The dry mass and dimensions were recorded, and the entire process was repeated for 10 cycles, or until the block broke down to the point it could not be tested. Photos of all the equipment, as well as the test set up will be included in the supplemental materials. Only two samples from each mix design could be allocated to take these measurements with one used to determine mass loss and the other to determine volume loss. This was done to provide the uniaxial compression test with enough samples to find an error value.

2.9 SEM sample preparation and setup

SEM imaging was taken to understand the overall morphology of rammed earth, search for signs of hydration products forming, and gain insight into the fiber matrix bonding. To generate the samples for these images, one of the 5% fiber filled cubes from the wet/dry cycling was crushed using the same setup as the compressive strength test. The specific cube was chosen due to the higher probability of finding a fiber bound to the matrix. A small piece broken off the interior of the sample was mounted to a SEM stub mount with carbon tape. Once mounted a gold coating was applied to prevent charge buildup on the surface. A Hitachi TM4000 desktop SEM was used with a 15 KeV acceleration
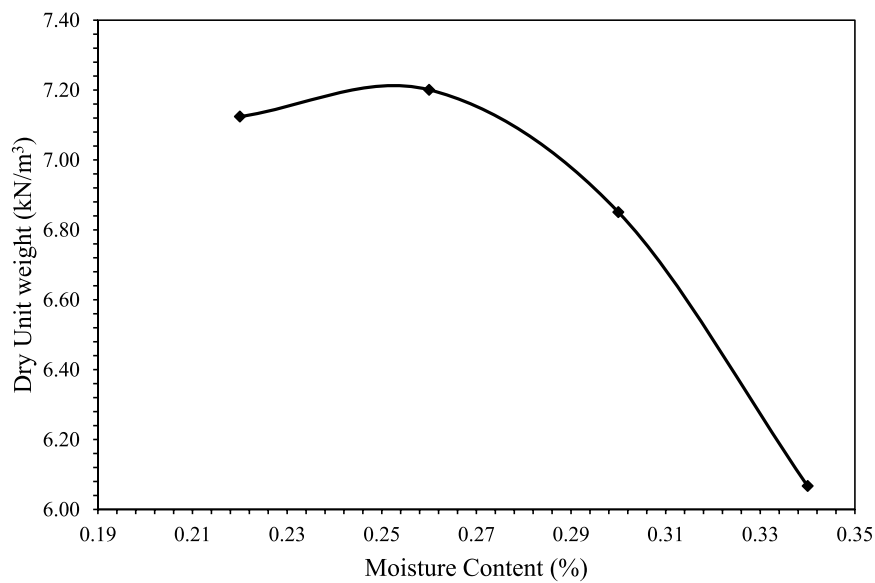
FIGURE 3
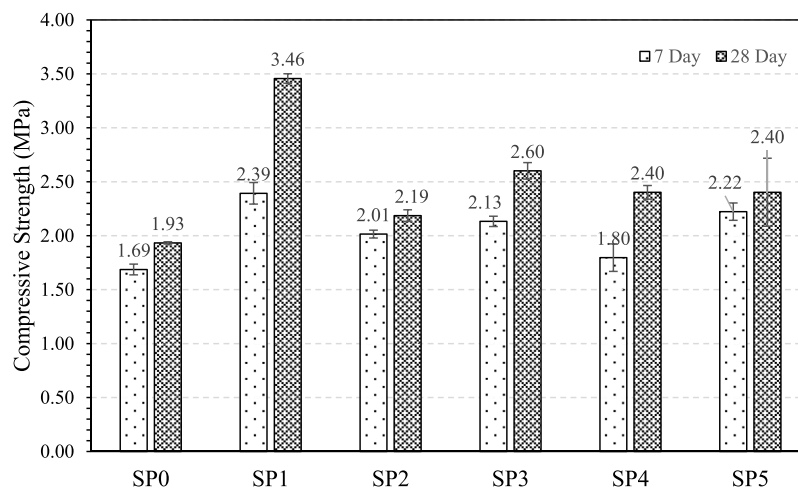Compaction characteristics of soil sample.

FIGURE 4
Compressive strength data of samples after 7- and 28-day air curing.

voltage for imaging. ×30 magnification was used to locate points of interest and further magnification, between 1500x and 2500x, was used to specific collect images.

3 Results and discussion

3.1 Optimum moisture content for soil compaction

The proctor test determines a relationship between the dry unit weight and the water content of the soil, known as the compaction curve. From the compaction curve, the optimum moisture content

that is required for the soil to attain maximum compaction can be determined. This is important when designing a mix design for a rammed earth block. If the moisture content is below the optimum values, the mixed material is stiff and has low workability. During compaction the low water content results in friction between the particles as they move past one another requiring more energy to achieve the same level of compaction. Above the optimum value the water begins to occupy the same space as the soil particles creating incompressible pockets in the material. At the optimum moisture content, the material is able to achieve a higher compaction volume while minimizing the energy required to do the compaction.

It can be observed from the compaction curve in Figure 3 that there is initially an increase of dry density with an increase in the
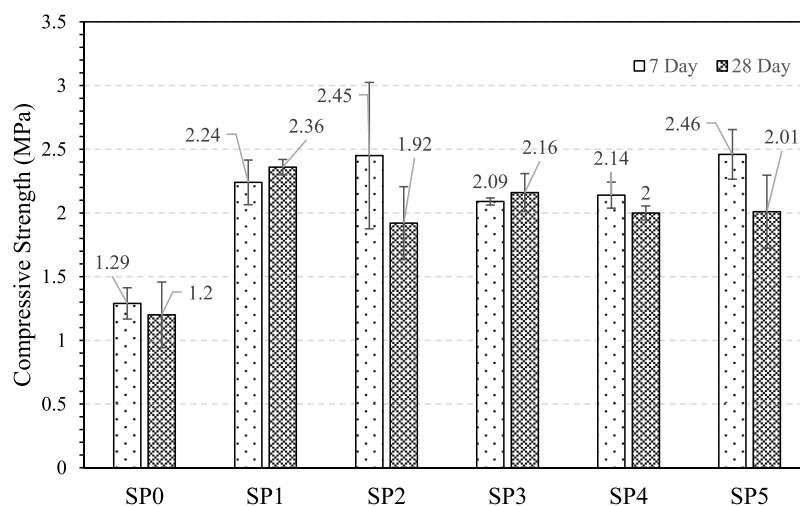
FIGURE 5
Compressive strength of samples after 7- and 28-day of curing in water.

water content. At a water content of 26%, a decrease in dry density is observed. The maximum peak of the soil compaction curve is at 7.20 kN · m/m³; this is the maximum dry density value.

3.2 Compressive strength of air-cured samples

Air cured compressive testing results are shown in Figure 4 with the 7-day average strength represented by the left bar and 28-day average strength drawn on the right. Error bars were calculated using a 95% confidence interval and average strengths written above their respective bars. In this data the control cubes had the lowest strength and the highest strength being shown by SP1. Overall, the strengths of all the samples remained higher than the control and had a very slight downward trend in compressive strength as fiber inclusion was increased. Another generalization is the low compressive strength of the material only maxing out at just below 3.5 MPa for SP1 cured in air. Looking at the highest reported dry compressive strengths of other studies the performance of the material explored in this study falls behind. While able to achieve a 0.16 MPa higher compressive strength compared to the barley fiber blocks in Giroudeon et al. (2019) the barley fiber blocks were not stabilized with Portland cement and had a 5% higher fiber content. Additionally in Raavi and Tripura, (2020a) the coir fiber blocks with 1% fiber and 10% stabilizer content had a compressive strength of 7.63 MPa. The lower compressive strength seen is likely due to the lower compaction energy used during the sample preparation step or a low fiber strength as compared to other studies. Increasing the compaction energy and standardizing the size and shape of the fibers could help to improve the performance of the material but would take more time and ultimately cost to sort the fibers and compress the blocks. While not varied the hydration products (CSH) helped stabilize the soil by interacting with the sand and gravel portions of the mix.

An observation that was not tested but noted during compaction is the effects of bridging fibers. In the samples with high fiber inclusion once the block was crushed past its ultimate failure stress large cracks formed in the body of the material and plate like components would break off the side faces. These plates would often remain attached to the main body of the material if a fiber bridged the crack body (Raavi and Tripura, 2020b; Rathod and Reddy, 2022). This maintained the overall shape of the sample even when it was not able to take more load.

3.3 Compressive strength of water-cured sample

The water cured compressive strength results with 7-day submersion and 28-day submersion testing shown as the left and right bars respectively in Figure 5. All the samples were cured in a relative humidity of 95% for 7 days prior to submersion and left undisturbed until compressive testing. Similar to the air cured testing the compressive strengths of the samples including fibers remained higher after the curing process than the control samples. However, a major difference is in the strength of the samples after 28 days of submersion with a loss in strength being seen in SP2, SP4, SP5, and the control. SP1 and SP3 only saw a minor gain in strength of roughly 0.1 MPa each. Variation in compressive strength in the same fiber inclusion amounts were also noted, leading to a higher deviation in the results.

The samples formed for this test were made in the same batch and mold as those used in the air cured testing. The increase in variation of the compressive strength would likely be caused by the water submersion rather than changes in the formation of the samples. During the compressive testing it was noted the surface dry samples still maintained a high degree of water in their interiors. Accompanying this was a visual decrease in volume without cracking as the soil was further compacted before the cube failed in compression. Loose soil was also found settled at the bottom of the water bucket after the submersion around each of the samples. This and the high variation could be due to a dissolution of the soil into the surrounding water resulting in a loss in soil compaction.

TABLE 5 Volume and mass change of samples after wet dry cycling.

Cycles	Volume loss (VL) and Mass loss (ML) each cycle											
	SP0		SP1		SP2		SP3		SP4		SP5	
	VL (cm³)	ML (g)	VL (cm³)	ML (g)	VL (cm³)	ML (g)	VL (cm³)	ML (g)	VL (cm³)	ML (g)	VL (cm³)	ML (g)
0	125.75	199.95	123.97	239.73	128.27	241.04	126.75	241.04	126.76	236.04	129.80	237.50
1	126.38	203.45	126.25	234.08	128.01	243.43	131.33	240.44	124.74	236.58	129.54	237.78
2	120.01	167.92	123.50	197.26	129.21	192.21	125.98	195.79	128.52	187.44	124.74	190.25
3	120.76	169.80	123.01	198.95	125.97	193.91	126.73	197.56	127.49	189.02	125.49	191.41
4	122.26	167.58	122.76	197.83	126.23	192.52	126.22	196.40	126.99	187.42	125.24	189.61
5	122.76	166.55	124.74	197.52	126.73	192.03	127.49	195.99	128.49	186.55	124.74	188.57
6	123.50	164.12	124.00	195.60	126.48	189.68	129.03	194.15	126.99	184.11	128.27	186.09
7	122.75	163.73	123.25	195.73	125.97	189.70	126.22	194.51	126.98	184.19	125.23	186.21
8	123.50	162.40	123.25	195.18	126.47	189.15	126.73	194.25	126.24	183.60	125.49	185.58
9	122.76	162.63	124.75	195.33	126.99	189.24	126.73	194.69	126.99	183.72	123.75	184.73
10	123.49	159.14	123.75	193.87	127.23	187.02	126.48	193.53	127.25	181.97	125.74	182.97
Total Change	−2.26	−40.81	−0.22	−45.86	−1.04	−54.02	−0.27	−47.51	0.49	−54.07	−4.06	−54.53
Change Excluding Cycles 0&1	3.48	−8.78	0.25	−3.39	−1.98	−5.19	0.50	−2.26	−1.27	−5.47	1.00	−7.28

3.4 Durability under wet and dry conditions

The wet dry cycling data is shown in Table 5, with the final change in the mass and volume of the cube samples after 10 cycles listed. The first two cycles (0&1) were removed in the calculations due to insufficient drying time leaving water in the interior of the sample. To address this after the second cycle the cubes were moved to a higher temperature oven (90°C–110°C) to fully remove water in the samples. The volume did not change appreciably after the increase in drying temperature between cycles 2 and 3. Volume stayed consistent across all the measurements with variation mainly being due to variation in where the caliper measurements were taken. Average volume and the changes in volume are shown in Table 5. The control sample had both the highest change in volume and mass, as well as a large degree of visual degradation at the end of cycling with large sections falling off during the drying stages.

The mass loss did not entirely correlate to the visual degradation of the samples due to any fibers falling off resulting in a volume loss but minimum mass loss. The largest mass loss was seen in the control with a drop in 8.78 g. This was followed up by the 5% fiber inclusion having 7.28 g of mass loss. The sample with the lowest mass loss was SP3 only losing 2.26 g, but this may not be consistent with the general trend seen in the other samples where mass loss should be roughly 5.2 g. The better performance could be due to better soil compaction or the lack of fibers at the surface to allow water into the interior of the sample. At the end of the cycling visual cracks started forming on the surface of the samples but overall, the cohesiveness of the cubes remained. Bridging fibers, similar to those seen in the compressive testing, connect the two crack surfaces and help hold the structure together. Because of the single sample used to

determine the mass and volume loss there will be an unknown error value for each measurement. Additional study with more samples will be needed to fully understand how the uncertainty between samples may effect these results.

3.5 SEM images and discussion

In the SEM images the material was shown to be a composite formed by a dried paste matrix surrounding stones and the plant fibers. This matrix is formed during the initial hydration and compaction process forming the stabilized rammed earth block. The fine clay, silt, and cement particles make up the bulk of the paste and once hydrated are allowed to shift and compact with one another. The cement reacts with local water in the environment and forms cement hydration products. The paste and aggregate interactions are shown in Figure 6. Interactions are not strong with the matrix separating from the aggregates as shown in Figure 6B. Additionally, Figure 6B shows failure of the binding material rather than the aggregates. This weakened matrix and poor bonding with aggregates may explain the overall poor compressive strength seen earlier.

At the interface of the plant fiber and the rammed earth several observations can be made regarding the low energy needed to remove the fiber from the block. Across the bulk of the fiber's edges separation can be seen with only a few regions of bonding occurring. Littered around the fiber in Figure 7A are shards of plant material that have broken off the main body. A higher magnification view of these fiber shards can be seen in Figure 7B, highlighted by point 2. Because of the fragile nature of the dried fibers if force is
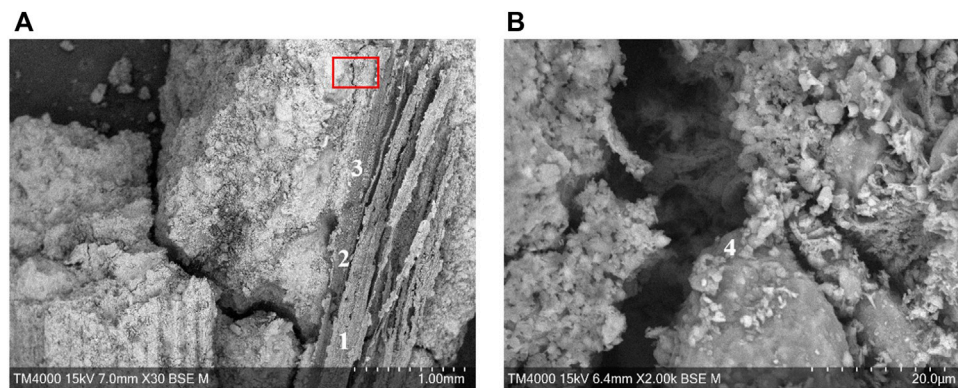
FIGURE 6
(A) ×30 magnified view of sample with a fiber bridging a crack at point 1. Moving up the fiber at point 2, the fiber has delaminated from the rammed earth while at point 3 there is still adhesion. The full fiber has seen damage along its full length with a majority of its integrity compromised; **(B)** 2500x magnified view of the red bound box, where the matrix has failed before the aggregate itself as seen at point 4.
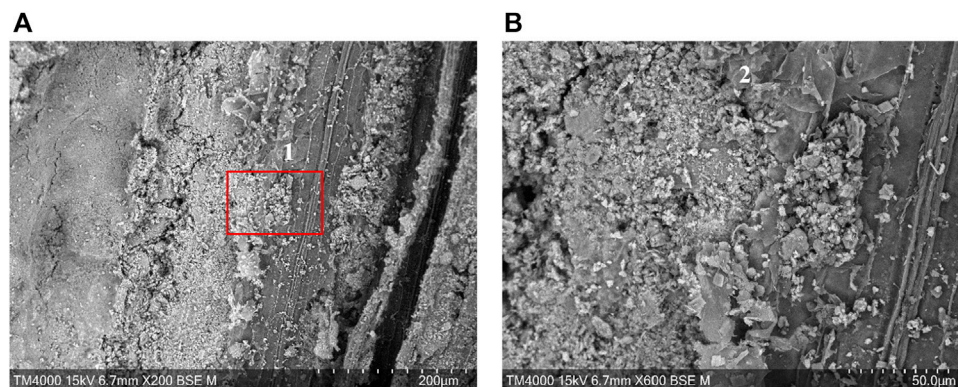

FIGURE 7
(A) Damaged plant fiber bound to the soil matrix material along its left edge at × 200 magnification. At point 1 the material is bound strongly to the matrix; **(B)** ×600 magnified view of the boxed area showing damage to the fiber edge with flakes of broken plant material scattered at point 2.

applied, the edges may fail debonding the bulk of the fiber. Bridging fibers can be seen in Figure 6A where the buffelgrass fiber, while damaged, is still bound to the matrix material providing some resistance to widening the crack body. In the work by Raavi and Tripura, (2020b) and Rathod and Reddy, (2022) plant fibers bridging the crack area and assisting in compressive strength were also highlighted in SEM imaging. One benefit seen at this interaction site is a greater abundance of hydrate products surrounding the fiber. One proposed reason is the fibers' ability to hold a large quantity of water acting as a reservoir for the Portland cement.

4 Conclusion

In this research, the incorporation of buffelgrass into a rammed earth-stabilized block for the enhancement of mechanical and durability properties was investigated. The study shows that the use of natural fiber reinforcing the material's compressive strength can be slightly increased without greatly increasing the bill of materials. For southern Arizona a

good candidate for this reinforcement is the invasive buffelgrass species. Using data from the GIS database, a suitable location for soil collection was found within 16 km of the Tucson area. The grass fibers were collected by the Pima County Natural Resources Parks & Recreation and processed by hand into consistent length fibers. Water content for optimum compaction was determined by the proctor test and particle size distribution was determined using a sieve analysis.

Air curing of the samples showed the highest consistency in measurement with a slight downward trend in compressive strength with increased fiber inclusion. Wet curing showed higher variation in compressive strength and reduced strength as submersion time increased. Both tests showed low compressive strength with most samples falling in the range of 2–3.5 MPa. While in the range of other studies this compressive strength is low posing a risk for use in high strength applications such as multistory building. In wet dry conditions the inclusion of fibers showed an improvement in mass loss and volume change compared to the control. However, higher fiber inclusion had diminishing returns on these properties. With both these results in mind, the mix design would be useful for low strength applications such as dirt trails or paths that are exposed to

short bursts of rain followed by long dry conditions. Additionally, the addition of buffelgrass fibers provides a low-cost natural fiber option to reinforce the rammed earth block and providing an outlet for buffelgrass clean up waste. Future research should include a look into the flexural strength of the material, increasing the compaction energy of during sample preparation, the long-term erosion characteristics, and exploring the interface between the fibers and the base material using SEM.

Data availability statement

The original contributions presented in the study are included in the article/supplementary material, further inquiries can be directed to the corresponding author.

Author contributions

FP: Investigation, Writing–original draft, Writing–review and editing. RF: Investigation, Writing–original draft. SK: Writing–review and editing. H-JK: Conceptualization, Funding acquisition, Methodology, Writing–review and editing, Writing–Original Draft. KD: Conceptualization, Resources, Writing–original draft.

Funding

Acknowledgments

Conflict of interest

The authors declare that the research was conducted in the absence of any commercial or financial relationships that could be construed as a potential conflict of interest.

Publisher's note

All claims expressed in this article are solely those of the authors and do not necessarily represent those of their affiliated organizations, or those of the publisher, the editors and the reviewers. Any product that may be evaluated in this article, or claim that may be made by its manufacturer, is not guaranteed or endorsed by the publisher.

References

ASTM (2020). D2487 standard Practice for classification of soils for engineering Purposes (unified soil classification System). Available at: https://www.astm.org/d2487-17e01.html.

ASTM (2021a). C109/C109M standard test method for compressive strength of hydraulic cement mortars (using 2-in. Or [50 mm] cube specimens). Available at: https://www.astm.org/c0109_c0109m-21.html.

ASTM (2021b). D698 standard test methods for laboratory compaction characteristics of soil using standard effort (12,400 ft-lbf/ft3 (600 kN-m/m3)). Available at: https://www.astm.org/d0698-12r21.html.

ASTM (2022). C150/C150M standard specification for Portland cement. Available at: https://www.astm.org/c0150_c0150m-22.html.

Bogas, J. A., Real, S., Cruz, R., and Azevedo, B. (2023). Mechanical performance and shrinkage of compressed earth blocks stabilised with thermoactivated recycled cement. J. Build. Eng. 79, 107892. doi:10.1016/J.JOBE.2023.107892

Editorial (2021). Concrete needs to lose its colossal carbon footprint. Nature 597 (7878), 593–594. doi:10.1038/D41586-021-02612-5

Elahi, T. E., Shahriar, A. R., and Islam, M. S. (2021). Engineering characteristics of compressed earth blocks stabilized with cement and fly ash. Constr. Build. Mater. 277, 122367. doi:10.1016/J.CONBUILDMAT.2021.122367

Giroudon, M., Laborel-Préneron, A., Aubert, J. E., and Magniont, C. (2019). Comparison of barley and lavender straws as bioaggregates in earth bricks. Constr. Build. Mater. 202, 254–265. doi:10.1016/J.CONBUILDMAT.2018.12.126

Javed, U., Khushnood, R. A., Memon, S. A., Jalal, F. E., and Zafar, M. S. (2020). Sustainable incorporation of lime-bentonite clay composite for production of ecofriendly bricks. J. Clean. Prod. 263, 121469. doi:10.1016/J.JCLEPRO.2020.121469

Koutous, A., and Hilali, E. (2023). Compression stress-strain curve of rammed earth: measuring and modelling. Results Eng. 18, 101012. doi:10.1016/J.RINENG.2023.101012

Laborel-Préneron, A., Aubert, J. E., Magniont, C., Tribout, C., and Bertron, A. (2016). Plant aggregates and fibers in earth construction materials: a review. Constr. Build. Mater. 111, 719–734. doi:10.1016/J.CONBUILDMAT.2016.02.119

Liu, L., Yao, Y., Zhang, L., and Wang, X. (2022). Study on the mechanical properties of modified rammed earth and the correlation of influencing factors. J. Clean. Prod. 374, 134042. doi:10.1016/J.JCLEPRO.2022.134042

Mañosa, J., Gómez-Carrera, A. M., Svobodova-Sedlackova, A., Maldonado-Alameda, A., Fernández-Jiménez, A., and Chimenos, J. M. (2022). Potential reactivity assessment of mechanically activated kaolin as alternative cement precursor. Appl. Clay Sci. 228, 106648. doi:10.1016/J.CLAY.2022.106648

Marshall, V. M., Lewis, M. M., and Ostendorf, B. (2012). Buffel grass (Cenchrus ciliaris) as an invader and threat to biodiversity in arid environments: a review. J. Arid Environ. 78, 1–12. doi:10.1016/J.JARIDENV.2011.11.005

Murugan, P. C., Saji Raveendran, P., Joseph Sekhar, S., Navaneethakrishnan, P., Beno Wincy, W., and Glivin, G. (2022). Investigation on the technical and economic benefits of implementing biomass gasifier in clay brick manufacturing industries. Sustain. Energy Technol. Assessments 53, 102554. doi:10.1016/J.SETA.2022.102554

Nshimiyimana, P., Fagel, N., Messan, A., Wetshondo, D. O., and Courard, L. (2020). Physico-chemical and mineralogical characterization of clay materials suitable for production of stabilized compressed earth blocks. Constr. Build. Mater. 241, 118097. doi:10.1016/J.CONBUILDMAT.2020.118097

Raavi, S. S. D., and Tripura, D. D. (2020a). Predicting and evaluating the engineering properties of unstabilized and cement stabilized fibre reinforced rammed earth blocks. *Constr. Build. Mater.* 262, 120845. doi:10.1016/J.CONBUILDMAT.2020.120845

Raavi, S. S. D., and Tripura, D. D. (2020b). Predicting and evaluating the engineering properties of unstabilized and cement stabilized fibre reinforced rammed earth blocks. *Constr. Build. Mater.* 262, 120845. doi:10.1016/J.CONBUILDMAT.2020.120845

Rathod, R. S. B., and Reddy, B. V. V. (2022). Behaviour of plain and fibre reinforced cement stabilised rammed earth under compression, tension and shear. *Constr. Build. Mater.* 344, 128125. doi:10.1016/J.CONBUILDMAT.2022.128125

Riza, F. V., and Rahman, I. A. (2015). The properties of compressed earth-based (CEB) masonry blocks. *Eco-Efficient Mason. Bricks Blocks Des. Prop. Durab.*, 379–392. doi:10.1016/B978-1-78242-305-8.00017-6

Skinder, B. M., Sheikh, A. Q., Pandit, A. K., and Ganai, B. A. (2014). Brick kiln emissions and its environmental impact: a Review. *J. Ecol. Nat. Environ.* 6 (1), 1–11. doi:10.5897/JENE2013.0423

Stazi, F., Nacci, A., Tittarelli, F., Pasqualini, E., and Munafò, P. (2016). An experimental study on earth plasters for earthen building protection: the effects of different admixtures and surface treatments. *J. Cult. Herit.* 17, 27–41. doi:10.1016/J.CULHER.2015.07.009

U.S. Department of the Interior (2010). War on buffelgrass. Available at: https://www.oi.gov/ocl/hearings/111/WarOnBuffelgrass_041010.

U.S. National Park Service (2023). Buffelgrass - Saguaro national Park. Available at: https://www.nps.gov/sagu/learn/nature/buffelgrass.htm.

Van Damme, H., and Houben, H. (2018). Earth concrete. Stabilization revisited. *Cem. Concr. Res.* 114, 90–102. doi:10.1016/J.CEMCONRES.2017.02.035

Venkatarama Reddy, B. V., and Prasanna Kumar, P. (2010). Embodied energy in cement stabilised rammed earth walls. *Energy Build.* 42 (3), 380–385. doi:10.1016/J.ENBUILD.2009.10.005

Wang, S., Gainey, L., Wang, X., Mackinnon, I. D. R., and Xi, Y. (2022). Influence of palygorskite on *in-situ* thermal behaviours of clay mixtures and properties of fired bricks. *Appl. Clay Sci.* 216, 106384. doi:10.1016/J.CLAY.2021.106384

Xin, Y., Robert, D., Mohajerani, A., Tran, P., and Pramanik, B. K. (2023). Energy efficiency of waste reformed fired clay bricks-from manufacturing to post application. *Energy* 282, 128755. doi:10.1016/J.ENERGY.2023.128755

Zami, M. S., Ewebajo, A. O., Baghabra Al-Amoudi, O. S., Al-Osta, M. A., and Mustafa, Y. M. H. (2022). Strength and durability improvement of cement-stabilized Al-Qatif soil by the addition of sand. *Arabian J. Geosciences* 15 (15), 1–12. doi:10.1007/S12517-022-10617-1